

GMRES Methods for Tomographic Reconstruction with an Unmatched Back Projector*

Per Christian Hansen[†] Ken Hayami[‡] Keiichi Morikuni[§]

P. C. Hansen and K. Morikuni dedicate this paper to K. Hayami.

Abstract

Unmatched pairs of forward and back projectors are common in X-ray CT computations for large-scale problems; they are caused by the need for fast algorithms that best utilize the computer hardware, and it is an interesting and challenging task to develop fast and easy-to-use algorithms for these cases. Our approach is to use preconditioned GMRES, in the form of the AB- and BA-GMRES algorithms, to handle the unmatched normal equations associated with an unmatched pair. These algorithms are simple to implement, they rely only on computations with the available forward and back projectors, and they do not require the tuning of any algorithm parameters. We show that these algorithms are equivalent to well-known LSQR and LSMR algorithms in the case of a matched projector. Our numerical experiments demonstrate that AB- and BA-GMRES exhibit a desired semi-convergence behavior that is comparable with LSQR/LSMR and that standard stopping rules work well. Hence, AB- and BA-GMRES are suited for large-scale CT reconstruction problems with noisy data and unmatched projector pairs.

Keywords: CT-reconstruction, regularizing iterations, AB-GMRES, BA-GMRES, semi-convergence, unmatched backprojector, unmatched normal equations, stopping rules

1 Introduction

Computational algorithms for X-ray computed tomography (CT) come in different forms. Some methods take their basis in an explicit formulation of the inverse operator, leading to the filtered back projection algorithm (for parallel-beam CT), the FDK algorithm (for cone-beam CT), etc. Other methods are based on a discretization of the problem followed by solving the – usually over- or underdetermined – linear system of equations by means of an iterative method. The latter approach, which is the basis for this work, is more general in the sense that it does not assume any specific scanning geometry, and it tends to produce better reconstructions in the case of limited-data and/or limited-angle problems [17].

CT reconstruction is an inverse problem where the forward problem refers to the mapping of the object’s linear attenuation coefficient to the data in the form of projections of the object onto the detector planes for various scan positions. In the case of 2D parallel-beam CT the forward operator is known as the Radon transform. Data consists of (noisy) measurements of the attenuation of the X-rays through the object, recorded in a set of detector elements. Discretization of this problem takes the form

$$Ax \approx b, \quad b = \bar{b} + e, \quad \bar{b} = A\bar{x}, \quad A \in \mathbb{R}^{m \times n}, \quad (1.1)$$

*We acknowledge financial support from Japan Society for the Promotion of Science grant no. S19008 and JP20K14356, and from The Villum Foundation through Villum Investigator grant no. 25893.

[†]Department of Applied Mathematics and Computer Science, Technical University of Denmark, pcha@dtu.dk

[‡]Professor Emeritus, National Institute of Informatics, hayami@nii.ac.jp

[§]Faculty of Engineering, Information and Systems, University of Tsukuba, Japan, morikuni@cs.tsukuba.ac.jp

where A is a discretization of the *forward projector*, b is the measured data, and x represents the reconstructed image of the object’s interior. Moreover, \bar{x} represents the exact object, \bar{b} represents the noise-free data, and e represents the measurement noise. A number of discretization schemes are available for computing the matrix A , see, e.g., [17, Chapter 9], [10] and [24, Appendix A]. A discussion of the noise in CT can be found in [17, Section 4.4]; here we assume that e is white Gaussian noise.

The matrix A is sparse and there are no restrictions on its dimensions m and n ; both overdetermined and underdetermined systems are used, depending on the measurement setup. In both cases it is common to consider a least squares solution which involves the normal equations in one of the forms

$$A^T A x = A^T b \quad \iff \quad \min_x \|b - A x\|_2$$

and

$$A A^T y = b, \quad x = A^T y \quad \iff \quad \min_x \|x\|_2 \quad \text{subject to} \quad A x = b.$$

The matrix A^T represents the so-called *back projector* which maps the data back onto the solution domain [27]. The back projector is a mathematical abstraction that has no physical interpretation, but it plays a central role in filtered back projection and many other reconstruction algorithms.

In large-scale CT problems, the matrix A – in spite of the fact that it is sparse – may be too large to store explicitly. Instead, one must use subroutines or functions that compute the multiplications with A and A^T in a matrix-free fashion, often using graphics processing units (GPUs) or other hardware accelerators. In order to make best use of this hardware and the memory hierarchy it is common to use different discretization techniques for the forward projector and the back projector [28]. This means that the matrix $B \in \mathbb{R}^{n \times m}$ which represents the back projector is typically different from the transpose A^T of the forward projector, and we say that B is an *unmatched back projector* or an *unmatched transpose*.

A consequence of this is that iterative solvers, which are supposed to solve the normal equations, instead solve the so-called *unmatched normal equations* in one of the forms

$$B A x = B b \quad \text{and} \quad A B y = b, \quad x = B y, \quad B \in \mathbb{R}^{n \times m}, \quad (1.2)$$

see [5] and [3] for details. The main drawback of using an unmatched transpose B is that the standard Simultaneous Iterative Reconstruction Technique (SIRT) iterative solvers (Landweber, Cimmino, CAV, DROP, SART) [16] do not converge when the iteration matrix $B A$ has one or more complex eigenvalues with a negative real part – which is very often the case in practice (see Figure 6.1 in Section 6.2). A convergence analysis of proximal gradient methods with an unmatched transpose is given in [2].

As shown in [3], one can modify the SIRT methods such that they solve a slightly modified problem whose iteration matrix has no eigenvalues with a negative real part, thus ensuring convergence. But this does introduce a (small) perturbation of the solution, and one must compute an estimate of the leftmost eigenvalue(s) of $B A$. In addition, the choice of a good relaxation parameter is nontrivial.

An alternative is to use Kaczmarz’s method [16] which does not explicitly involve the matrix transpose; but this method has other drawbacks. In its original form, Kaczmarz’s method operates on a single row of A at a time, which is unsuited for modern computer architectures. Block versions [30] have better performance but they require a good choice of the blocks, the blocks may be unmatched, and again the choice of a good relaxation parameter is nontrivial.

The present work explores an alternative approach, where we use the well-known GMRES algorithm to solve the unmatched normal equations (1.2) with an unmatched back projector. Thus, we avoid introducing a perturbation as well as the need for eigenvalue computations for the sake of ensuring convergence of the SIRT methods, and we avoid the choice of the relaxation

parameter. This makes it easier to develop a black-box CT solver that does not rely on the user’s knowledge of convergence criteria, eigenvalue computations, etc. Our work is based on previous work on the preconditioned AB- and BA-GMRES methods for solving least squares problems [19] and here we explicitly demonstrate the successful use of these methods for the CT reconstruction problems.

The main goal of our work is to study the performance and the regularizing effects of the AB- and BA-GMRES algorithms when applied to CT reconstruction problems. To do this, we deliberately commit “inverse crime” and generate the noise-free data as $\bar{b} = A \bar{x}$, meaning that the same model (the matrix A) is used to generate and reconstruct the data. To determine which unmatched pair is preferable, one must use real (or carefully simulated) data to avoid the inverse crime – this is a topic for future research.

We remark that an alternative to using the unmatched transpose is to use Kaczmarz’s method as preconditioner (i.e., for B) in the AB- and BA-GMRES algorithms, as described and analyzed in [25, 4]. We shall not pursue that approach here, but leave it for future work.

Our paper is organized as follows. In Section 2 we summarize the AB- and BA-GMRES algorithms, and in Section 3 we present new first-order perturbation theory for the unmatched normal equations. The behavior of the iterative methods in the presence of noisy data is discussed in Section 4, and in Section 5 we study the regularizing properties of AB- and BA-GMRES when $B = A^\top$. Finally, in Section 6 we present a number of numerical examples that illustrate our theory and the performance of the AB- and BA-GMRES algorithms. We use the following notation: $\mathcal{R}(\cdot)$ denotes the range of a matrix, $\mathcal{N}(\cdot)$ denotes the null space of a matrix. For Krylov subspaces we use the notation

$$\mathcal{K}_k(M, d) = \text{span}\{d, Md, M^2d, \dots, M^{k-1}d\}.$$

Moreover, $v|_{\mathcal{S}}$ denotes the orthogonal projection of vector v on the subspace \mathcal{S} , and $\sigma_i(A)$ denotes the i th singular value of A .

2 The AB-GMRES and BA-GMRES Algorithms

The two algorithms AB-GMRES and BA-GMRES were originally presented and analyzed in [19] as alternative methods for solving linear least squares problems $\min_{x \in \mathbb{R}^n} \|b - Ax\|_2$ according to the following principles:

- AB-GMRES solves $\min_{y \in \mathbb{R}^m} \|b - AB y\|_2$, $x = B y$ with $B \in \mathbb{R}^{n \times m}$ as a right preconditioner.
- BA-GMRES solves $\min_{x \in \mathbb{R}^n} \|B b - B A x\|_2$ with $B \in \mathbb{R}^{n \times m}$ as a left preconditioner.

Here we briefly summarize these algorithms using the notation $H_k = (h_{ij}) \in \mathbb{R}^{(k+1) \times k}$ and $e_1 = (1, 0, \dots, 0)^\top \in \mathbb{R}^{k+1}$; we describe some stopping rules later in Section 6.4.

Algorithm AB-GMRES

```

Choose initial  $x_0$ 
 $r_0 = b - A x_0$ 
 $w_1 = r_0 / \|r_0\|_2$ 
for  $k = 1, 2, \dots$ 
     $q_k = AB w_k$ 
    for  $i = 1, 2, \dots, k$ 
         $h_{i,k} = q_k^\top w_i$ 
         $q_k = q_k - h_{i,k} w_i$ 
    endfor
 $h_{k+1,k} = \|q_k\|_2$ 

```

Algorithm BA-GMRES

```

Choose initial  $x_0$ 
 $r_0 = B b - B A x_0$ 
 $w_1 = r_0 / \|r_0\|_2$ 
for  $k = 1, 2, \dots$ 
     $q_k = B A w_k$ 
    for  $i = 1, 2, \dots, k$ 
         $h_{i,k} = q_k^\top w_i$ 
         $q_k = q_k - h_{i,k} w_i$ 
    endfor
 $h_{k+1,k} = \|q_k\|_2$ 

```

| | |
|---|---|
| $w_{k+1} = q_k/h_{k+1,k}$ | $w_{k+1} = q_k/h_{k+1,k}$ |
| $y_k = \arg \min_y \ \ r_0\ _2 e_1 - H_k y \ _2$ | $y_k = \arg \min_y \ \ r_0\ _2 e_1 - H_k y \ _2$ |
| $x_k = x_0 + B [w_1, w_2, \dots, w_k] y_k$ | $x_k = x_0 + [w_1, w_2, \dots, w_k] y_k$ |
| $r_k = b - A x_k$ | $r_k = b - A x_k$ |
| stopping rule goes here | stopping rule goes here |
| endfor | endfor |

The following statements about the convergence are from [19]. We emphasize that the two methods use the same Krylov subspace $\mathcal{K}_k(BA, Bb)$ for the solution, but they use different objective functions.

AB-GMRES

- AB-GMRES applies GMRES to $\min_u \|b - ABu\|_2$, $x = Bu$, i.e., forms the iterates $u_k \in u_0 + \mathcal{K}_k(AB, b)$ that minimize $\|b - ABu\|_2$, i.e., $x_k \in x_0 + \mathcal{K}_k(BA, Bb)$ that minimize $\|b - Ax\|_2$.
- The equality $\min_x \|b - Ax\|_2 = \min_z \|b - ABz\|_2$ holds for all $b \in \mathbb{R}^m$ if and only if $\mathcal{R}(AB) = \mathcal{R}(A)$ [19, Theorem 3.1]. Note that $\mathcal{R}(AB) = \mathcal{R}(A)$ holds if $\mathcal{R}(B) = \mathcal{R}(A^\top)$ [19, Lemma 3.3].
- If $\mathcal{R}(B) = \mathcal{R}(A^\top)$, then AB-GMRES determines a solution of $\min_x \|b - Ax\|_2$ without breakdown for all $b \in \mathbb{R}^m$ if and only if $\mathcal{R}(B^\top) = \mathcal{R}(A)$ [19, Corollary 3.8].

BA-GMRES

- BA-GMRES applies GMRES to $\min \|Bb - BAx\|_2$, i.e., forms the iterates $x_k \in x_0 + \mathcal{K}_k(BA, Bb)$ that minimize $\|Bb - BAx\|_2$.
- The problems $\min_x \|b - Ax\|_2$ and $\min_x \|Bb - BAx\|_2$ are equivalent for all $b \in \mathbb{R}^m$ if and only if $\mathcal{R}(B^\top BA) = \mathcal{R}(A)$ [19, Theorem 3.11]. Note that $\mathcal{R}(B^\top BA) = \mathcal{R}(A)$ holds if $\mathcal{R}(B^\top) = \mathcal{R}(A)$ [19, Lemma 3.14].
- If $\mathcal{R}(B^\top) = \mathcal{R}(A)$ and $\mathcal{R}(B) \cap \mathcal{N}(A) = \{0\}$, then BA-GMRES determines a solution of $\min_x \|b - Ax\|_2$ without breakdown for all $b \in \mathbb{R}^m$ [25, Theorem 3.1].

The conditions on the ranges $\mathcal{R}(AB) = \mathcal{R}(A)$ and $\mathcal{R}(B^\top BA) = \mathcal{R}(A)$ ensure the equivalence between the matched and unmatched normal equations, as seen above. Simply, $\mathcal{R}(B) = \mathcal{R}(A^\top)$ implies $\mathcal{R}(AB) = \mathcal{R}(A)$ and $\mathcal{R}(B^\top) = \mathcal{R}(A)$ implies $\mathcal{R}(B^\top BA) = \mathcal{R}(A)$. Further, these conditions also ensure the convergence of AB- and BA-GMRES. However, it is not easy to check if these conditions are satisfied in practice.

If $B \approx A^\top$, solving the unmatched normal equations by using AB- and BA-GMRES we expect to obtain an approximation to the solution. This expectation can be supported by the observation that if B is close to A^\top , then $\mathcal{R}(B)$ and $\mathcal{R}(B^\top)$ can be close to $\mathcal{R}(A^\top)$ and $\mathcal{R}(A)$, respectively, e.g., the principal angles between the pair of the ranges $\mathcal{R}(B)$ and $\mathcal{R}(A^\top)$ and pair $\mathcal{R}(B^\top)$ and $\mathcal{R}(A)$ can be small from the extended $\sin \theta$ theorem [34, Section 3], [31, Chapter 2]

$$\left(\left\| \sin \theta(\mathcal{R}(B), \mathcal{R}(A^\top)) \right\|^2 + \left\| \sin \theta(\mathcal{R}(B^\top), \mathcal{R}(A)) \right\|^2 \right)^{1/2} \leq \frac{\sqrt{2} \|B - A^\top\|}{\max(\sigma_r(A), \sigma_r(B))},$$

where $\|\cdot\|$ is either the 2-norm or the Frobenius norm and we assume that $r = \text{rank}(A) = \text{rank}(B)$. Moreover, $\sin \theta(\mathcal{S}, \mathcal{T}) = \text{diag}(\sin \theta_1, \sin \theta_2, \dots, \sin \theta_r)$ is a diagonal matrix with the principal angles $\theta_1 \geq \theta_2 \geq \dots \geq \theta_r$ between subspaces \mathcal{S} and \mathcal{T} with $r = \dim \mathcal{S} = \dim \mathcal{T}$. In case of the matrix 2-norm, we can instead use the upper bound

$$\sqrt{2} \min \left(\kappa_2(A) \frac{\|B - A^\top\|_2}{\|A\|_2}, \kappa_2(B) \frac{\|B - A^\top\|_2}{\|B\|_2} \right).$$

3 First-Order Perturbation Theory

To further motivate the use of the unmatched normal equations, we consider the difference between the solutions of the matched and unmatched normal equations, and we study how this difference depends on the unmatchedness of the pair (A, B) .

A first-order perturbation analysis for the unmatched normal equations was given in [5, Section 2.1]. Their analysis gave a bound for the distance between the closest pair of a point in the solution set of the least squares problem $\min_{x \in \mathbb{R}^n} \|b - Ax\|_2$ and a point in the solution set of its perturbed problem. Here, we perform an alternative first-order perturbation analysis specifically for the minimum-norm solutions, as discussed below. This analysis refines the previous perturbation analysis in [5, Section 2.1].

Generally, we can assume to have modeling error also in A , in addition to B . Let A and \bar{b} be the ideal model and data, respectively, and let

$$\tilde{A} = A + E_1, \quad \tilde{B} = A^\top + E_2^\top, \quad b = \bar{b} + \delta b$$

be the perturbed models and data. Moreover, let \bar{x} be a ground truth solution of $\min_{x \in \mathbb{R}^n} \|b - Ax\|_2$ and $\bar{r} = \bar{b} - A\bar{x}$ be the corresponding least squares residual, for which $A^\top \bar{r} = 0$ holds. The perturbed matrices \tilde{A} and \tilde{B} can be regarded as A and B in the unmatched normal equations (1.2).

Now, consider solving the perturbed unmatched normal equations

$$\tilde{B} \tilde{A} (x_{\min} + \delta x_{\min}) = \tilde{B} b, \quad (3.1)$$

where x_{\min} denotes the minimum-norm solution of the unperturbed normal equations $A^\top A x = A^\top b$. Note that the linear system (3.1) is consistent if $\tilde{B} b \in \mathcal{R}(\tilde{B} \tilde{A})$. Irrespective of the inconsistency of (3.1), the minimum-norm solution of the least squares problem

$$\min_{x_{\min} + \delta x_{\min} \in \mathbb{R}^n} \|\tilde{B} b - \tilde{B} \tilde{A} (x_{\min} + \delta x_{\min})\|_2 \quad (3.2)$$

is given by $(\tilde{B} \tilde{A})^\dagger \tilde{B} b$, where \dagger denotes the Moore-Penrose generalized inverse (pseudoinverse). We are concerned with the difference between the minimum-norm solution of $\min_{x \in \mathbb{R}^n} \|b - Ax\|_2$ and the minimum-norm solution $x_{\min} + \delta x_{\min}$ of (3.2). Note that the solution of interest in (1.1) is not necessarily the minimum-norm solution but may lie close to it.

Theorem 3.1. *Assume that \tilde{A} and \tilde{B} are both acute perturbations of A and A^\top , respectively, i.e.,*

$$\|P_{\mathcal{R}(\tilde{A})} - P_{\mathcal{R}(A)}\|_2 < 1, \quad \|P_{\mathcal{R}(\tilde{A}^\top)} - P_{\mathcal{R}(A^\top)}\|_2 < 1$$

and

$$\|P_{\mathcal{R}(\tilde{B})} - P_{\mathcal{R}(A^\top)}\|_2 < 1, \quad \|P_{\mathcal{R}(\tilde{B}^\top)} - P_{\mathcal{R}(A)}\|_2 < 1,$$

respectively, where $P_{\mathcal{S}}$ denotes the orthogonal projection onto a subspace \mathcal{S} . Then, the first-order bound of the relative error norm is given by

$$\frac{\|\delta x_{\min}\|_2}{\|x_{\min}\|_2} \leq \kappa_2(A) \left[\sigma_r^{-1} \left(2\|E_1\|_2 \frac{\|\bar{b}|_{\mathcal{R}(A)}\|_2}{\|\bar{b}\|_2} + \|E_2\|_2 \frac{\|\bar{b}|_{\mathcal{R}(A)^\perp}\|_2}{\|\bar{b}\|_2} \right) + \frac{\|\delta b|_{\mathcal{R}(A)}\|_2}{\|\bar{b}\|_2} \right],$$

where σ_r denotes the smallest nonzero singular value of A and $\kappa_2(A) = \|A\|_2/\sigma_r$ is the condition number of A .

See Appendix A for the proof. This theorem shows that the error bound depends linearly on $\|E_1\|$, $\|E_2\|$, $\|\bar{b}|_{\mathcal{R}(A)}\|$, $\|\bar{b}|_{\mathcal{R}(A)^\perp}\|$ and $\|\delta b|_{\mathcal{R}(A)}\|$, whereas the bound is independent of $\delta b|_{\mathcal{R}(A)^\perp}$. If the smallest nonzero singular value σ_r is very small, then the perturbations E_1 and E_2 can greatly affect the error.

The first-order bound of the relative error norm in the ‘‘inverse crime’’ case, where $\bar{b} = A\bar{x}$ with the minimum-norm solution $\bar{x} = x_{\min}$ and hence $\bar{r} = 0$, is given as follows.

Corollary 3.2. *Assume that $E_1 = 0$, \tilde{B} is an acute perturbations of A^\top , and $\bar{b}|_{\mathcal{R}(A)^\perp} = 0$. Then, the first-order bound of the relative error norm is given by*

$$\frac{\|\delta x_{\min}\|_2}{\|x_{\min}\|_2} \leq \kappa_2(A) \frac{\|\delta b|_{\mathcal{R}(A)}\|_2}{\|\bar{b}\|_2}.$$

This corollary follows directly from Theorem 3.1 and shows that the error bound is independent of E_2 and $\delta b|_{\mathcal{R}(A)^\perp}$ in the “inverse crime” case. Note that the higher-order terms of these quantities, such as $E_2^T \delta b$, can contribute to the error.

The above analysis focuses on the unmatched normal equations that BA-GMRES deals with. A first-order perturbation analysis for the unmatched normal equations $\tilde{A}\tilde{B}y = b$, $x = \tilde{B}y$ that AB-GMRES deals with in the consistent case $b \in \mathcal{R}(\tilde{A}\tilde{B})$ is performed in [5, section 2.2]. The corresponding analysis in the inconsistent case $b \notin \mathcal{R}(\tilde{A}\tilde{B})$ is left open.

4 Iterative Regularization and Semi-Convergence

When we discretize an inverse problem we obtain a coefficient matrix A whose nonzero singular values decay gradually to zero with no gap anywhere, and A has a large condition number. Therefore, it is not a good idea to naively solve the problem (1.1) with noisy data. With the notation from (1.1) and assuming that the exact solution \bar{x} satisfies

$$\bar{x} = A^\dagger \bar{b} \in \mathcal{R}(A^\top),$$

the minimum-norm least squares solution to the noisy problem has the form $A^\dagger b = \bar{x} + A^\dagger e$. Here, the second term $A^\dagger e$ is highly undesired because – due to the large condition number of A – it has elements that are much larger than those in \bar{x} . We need to use a regularization method that filters the influence from the noise.

The singular value decomposition (SVD) provides a convenient framework for analyzing this situation. Let the coefficient matrix A in (1.1) have the SVD

$$A = U \Sigma V^\top = \sum_{i=1}^r u_i \sigma_i v_i^\top, \quad \sigma_1 \geq \sigma_r \geq \dots \geq \sigma_r > 0, \quad r = \text{rank}(A)$$

with

$$U = [u_1, u_2, \dots, u_r] \in \mathbb{R}^{m \times r}, \quad \Sigma = \text{diag}(\sigma_i) \in \mathbb{R}^{r \times r}, \quad V = [v_1, v_2, \dots, v_r] \in \mathbb{R}^{n \times r}.$$

Then we can write the minimum-norm least squares solution as

$$A^\dagger b = \bar{x} + A^\dagger e = \sum_{i=1}^r \frac{u_i^\top \bar{b}}{\sigma_i} v_i + \sum_{i=1}^r \frac{u_i^\top e}{\sigma_i} v_i. \quad (4.1)$$

Discretizations of inverse problems satisfy the *discrete Picard condition* (DPC) meaning that, in average, the absolute values $|u_i^\top \bar{b}|$ decay faster than the singular values [15, Section 3.3]. The first term in (4.1) is equal to the exact, noise-free solution $\bar{x} = A^\dagger \bar{b}$ and the DPC ensures that its norm stays bounded as the problem size increases. If e is white noise then so is $U^\top e$ meaning that the coefficients $u_i^\top e / \sigma_i$ will, on average, increase due to the decreasing singular values. Consequently, the second term in (4.1) is typically much larger than the first term – and its norm increases with the problem size. All regularization methods essentially filter or dampen the SVD components corresponding to the smaller singular values, thus reducing the influence of the noise and, at the same time, computing a good approximation to \bar{x} .

The key mechanism behind the use of *iterative solvers* for computing solutions to inverse problems with noisy data, such as the CT reconstruction problem, is known as *semi-convergence* [15, Chapter 6]. When we apply an iterative method (typically a least squares solver) to the noisy problem (1.1) then the reconstruction error $\|\bar{x} - x_k\|_2$, where x_k denotes the k th iterate, exhibits two different phases:

1. During the initial iterations $\|\bar{x} - x_k\|_2$ decreases and x_k appears to approach the ground truth \bar{x} .
2. After a while $\|\bar{x} - x_k\|_2$ starts to increase, and asymptotically x_k converges to the undesired least squares solution.

To obtain a meaningful regularized solution we must stop the iterations at the transition point where the iteration vector x_k is as close to \bar{x} as possible. Development of stopping rules that seek to terminate the iterations at this point are closely related to methods for choosing regularization parameters (see, e.g., [17, Chapter 5] and [29]); overviews of stopping rules in the context of CT are given in [17, Section 11.2] and [18].

Deeper insight into the semi-convergence, and explanations when and why it manifests itself, has been a topic of research for many years. For methods where x_k can be expressed as a filtered SVD solution of the form

$$x_k = \sum_{i=1}^r \phi_i^{(k)} \frac{u_i^\top b}{\sigma_i} v_i, \quad \phi_i^{(k)} = \text{filter factor at } k\text{th iteration}, \quad (4.2)$$

we have a good understanding, see, e.g., [17] and [15, Chapter 6]. For example, for the Landweber iteration $x_k = x_{k-1} + \omega A^\top (b - Ax_{k-1})$ with relaxation parameter ω we have $\phi_i^{(k)} = 1 - (1 - \omega \sigma_i^2)^k$, and for CGLS the filters $\phi_i^{(k)}$ can be expressed as polynomials of degree k that depend on the Ritz values associated with the k th CGLS iteration, cf. [13, Section 6.4.3].

For other methods where x_k cannot easily be expressed in terms of the SVD the understanding is less mature (see [6], [33] for emerging insight into Kaczmarz’s method). The analysis of the regularizing properties of GMRES applied to $Ax = b$ is complicated by the fact that it is connected to the convergence of the Ritz values of the underlying Arnoldi algorithm.

- The insight obtained from [1] is that if the noise-free data \bar{b} lies in a finite-dimensional Krylov subspace, and if GMRES is equipped with a suitable stopping rule, then the GMRES-solution converges to the exact solution \bar{x} as the noise goes to zero.
- The focus of [9] is so-called “hybrid methods” where regularization is applied to the Hessenberg systems in GMRES, but the main result in [9, §3.1.2] applies more generally: Assume that the system in (1.1) satisfies the DPC and that the left singular vectors of the Hessenberg matrices of two consecutive GMRES steps, applied to $Ax = b$, resemble each other – then the Hessenberg systems in GMRES also satisfy the DPC.

Taken together, these results imply that if all the SVD components corresponding to the larger singular values are captured in order of decreasing magnitude, when GMRES is applied to $Ax = b$, then GMRES will exhibit semi-convergence. Unfortunately, a complete understanding of these aspects has not emerged yet. Hence, while the semi-convergence aspect of GMRES is crucial in this work, we primarily rely on insight obtained from numerical experiments.

5 The Regularizing Properties of AB- and BA-GMRES with a Matched Transpose

To understand the regularizing properties of the AB- and BA-GMRES methods when $B \approx A^\top$, let us consider the limiting case when $B = A^\top$ (the matched case).

5.1 The AB-GMRES Algorithm with $B = A^\top$

The k th step of AB-GMRES with $B = A^\top$ solves

$$\min_{u \in u_0 + \mathcal{K}_k(AA^\top, r_0)} \|b - AA^\top u\|_2^2$$

and it determines the k th iterate where $x_k = A^\top u_k$. Hence,

$$x_k = A^\top u_k = A^\top u_0 + A^\top \mathcal{K}_k(AA^\top, r_0) = x_0 + \mathcal{K}_k(A^\top A, A^\top r_0) .$$

The method minimizes

$$\|r_k\|_2^2 = \|r_k|_{\mathcal{R}(A)}\|_2^2 + \|r_k|_{\mathcal{R}(A)^\perp}\|_2^2 ,$$

where

$$r_k = b - Ax_k = b|_{\mathcal{R}(A)} + b|_{\mathcal{R}(A)^\perp} - Ax_k = r_k|_{\mathcal{R}(A)} + b|_{\mathcal{R}(A)^\perp}$$

and

$$r_k|_{\mathcal{R}(A)} = b|_{\mathcal{R}(A)} - Ax_k , \quad r_k|_{\mathcal{R}(A)^\perp} = b|_{\mathcal{R}(A)^\perp} .$$

Hence, the method minimizes $\|r_k|_{\mathcal{R}(A)}\|_2^2$. In summary, the AB-GMRES method with $B = A^\top$ minimizes $\|r_k|_{\mathcal{R}(A)}\|_2^2$, and its iterates satisfy $x_k \in x_0 + \mathcal{K}_k(A^\top A, A^\top r_0)$.

5.2 The LSQR Algorithm

Next, consider the LSQR algorithm for $\min_x \|b - Ax\|_2$ which is mathematically equivalent to the CGLS method. Note

$$\min_x \|b - Ax\|_2 \iff A^\top Ax = A^\top b \iff A^\top r = 0 , \quad (5.1)$$

where $r = b - Ax$. The LSQR and CGLS methods are mathematically equivalent to applying the Conjugate Gradient (CG) method to the normal equations $A^\top Ax = A^\top b$. They minimize $\varepsilon^\top A^\top A \varepsilon = (A\varepsilon)^\top A\varepsilon = \|A\varepsilon\|_2^2$, where $\varepsilon = x - x^*$ and x^* is any solution of (5.1). Note

$$A\varepsilon = A(x - x^*) = Ax - Ax^* = (b - Ax^*) - (b - Ax) = r^* - r ,$$

where

$$r^* = b - Ax^* , \quad r = b - Ax .$$

Also note

$$r = b - Ax = b|_{\mathcal{R}(A)} - Ax + b|_{\mathcal{R}(A)^\perp} = r|_{\mathcal{R}(A)} + r|_{\mathcal{R}(A)^\perp} ,$$

where

$$r|_{\mathcal{R}(A)} = b|_{\mathcal{R}(A)} - Ax^* , \quad r|_{\mathcal{R}(A)^\perp} = b|_{\mathcal{R}(A)^\perp} ,$$

and

$$r^* = b - Ax^* = b|_{\mathcal{R}(A)} - Ax^* + b|_{\mathcal{R}(A)^\perp} = r^*|_{\mathcal{R}(A)} + r^*|_{\mathcal{R}(A)^\perp} ,$$

where

$$r^*|_{\mathcal{R}(A)} = b|_{\mathcal{R}(A)} - Ax^* , \quad r^*|_{\mathcal{R}(A)^\perp} = b|_{\mathcal{R}(A)^\perp} .$$

Hence,

$$0 = A^\top r^* = A^\top (r^*|_{\mathcal{R}(A)} + r^*|_{\mathcal{R}(A)^\perp}) = A^\top r^*|_{\mathcal{R}(A)} ,$$

where $\mathcal{R}(A)^\perp = \mathcal{N}(A^\top)$. Hence, $r^*|_{\mathcal{R}(A)} = 0$. Thus we have

$$A\varepsilon = r^* - r = r^*|_{\mathcal{R}(A)} - r|_{\mathcal{R}(A)} = -r|_{\mathcal{R}(A)}$$

and

$$\|A\varepsilon\|_2^2 = \|r|_{\mathcal{R}(A)}\|_2^2 .$$

Thus, CGLS minimizes $\|r_k|_{\mathcal{R}(A)}\|_2^2$, where $r_k = b - Ax_k$. The iterates satisfy $x_k \in x_0 + \mathcal{K}_k(A^\top A, A^\top r_0)$.

Therefore, AB-GMRES with $B = A^\top$, as well as LSQR and CGLS for $\min_x \|b - Ax\|_2$, minimize $\|r_k|_{\mathcal{R}(A)}\|_2^2$, where $r_k = b - Ax_k$, and the iterates (solutions) are in the same space, i.e., $x_k \in x_0 + \mathcal{K}_k(A^\top A, A^\top r_0)$. Thus, these methods are mathematically equivalent.

In finite precision arithmetic, AB-GMRES with $B = A^\top$ should be numerically more stable than CGLS and LSQR, since AB-GMRES is based on the Arnoldi process whereas LSQR and CGLS rely on short-term recurrences. In fact, AB-GMRES may be numerically equivalent to LSQR and CGLS with full reorthogonalization [19], and this is confirmed by our numerical experiments (which are not included here).

Now, it is well known that CGLS has good regularizing properties for discrete ill-posed problems, leading to semi-convergence, see, e.g. [15, 11, 12, 22]. When $B \approx A^\top$, we may still apply AB-GMRES, while applying LSQR (which is equivalent to applying CG to the unmatched normal equations $BAx = Bb$) is not well founded and may be problematic since BA is neither symmetric nor positive semi-definite. Also, we may still expect semi-convergence of AB-GMRES, as will be demonstrated in the numerical experiments. Specifically, in Section 6.6 we study experimentally how semi-convergence is influenced by the difference between B and A^\top .

5.3 The BA-GMRES Algorithm with a Matched Transpose

BA-GMRES applies GMRES to $\min_x \|Bb - BAx\|_2$. It minimizes $\|Br_k\|_2^2$ where $r_k = b - Ax_k$, and

$$x_k \in x_0 + \mathcal{K}_k(BA, Br_0) = x_0 + B\mathcal{K}_k(AB, r_0).$$

BA-GMRES with $B = A^\top$ applies GMRES to $\min_x \|A^\top b - A^\top Ax\|_2$. It minimizes

$$\|A^\top r\|_2^2 = (A^\top r)^\top A^\top r = r^\top AA^\top r,$$

where

$$r = b - Ax = r|_{\mathcal{R}(A)} + r|_{\mathcal{R}(A)^\perp} \quad \text{and} \quad r|_{\mathcal{R}(A)} = b|_{\mathcal{R}(A)} - Ax, \quad r|_{\mathcal{R}(A)^\perp} = b|_{\mathcal{R}(A)^\perp}.$$

Thus,

$$A^\top r = A^\top (r|_{\mathcal{R}(A)} + r|_{\mathcal{N}(A^\top)}) = A^\top r|_{\mathcal{R}(A)}$$

and BA-GMRES with $B = A^\top$ minimizes $\|A^\top r|_{\mathcal{R}(A)}\|_2^2$. The iterates satisfy

$$x_k = x_0 + \mathcal{K}_k(A^\top A, A^\top r_0) = x_0 + A^\top \mathcal{K}_k(AA^\top, r_0).$$

BA-GMRES with $B = A^\top$ applies GMRES to

$$A^\top Ax = A^\top b \quad \iff \quad \min_{x \in \mathbb{R}^n} \|b - Ax\|_2,$$

which is mathematically equivalent to applying MINRES to the normal equations $A^\top Ax = A^\top b$, and which is equivalent to LSMR [8]. Again, BA-GMRES with $B = A^\top$ should be numerically more stable than LSMR. It may be numerically equivalent to LSMR with full reorthogonalization, and again our numerical experiments (not included here) confirm this.

Similar to CGLS, LSMR also has good regularizing properties when applied to discrete ill-posed problems [8, 23]. We may still apply BA-GMRES when $B \approx A^\top$, while it is not well founded to apply LSMR since BA is no longer symmetric and we cannot apply MINRES to $BAx = Bb$. We expect that BA-GMRES exhibits semi-convergence, as will be demonstrated in the numerical experiments.

6 Numerical Examples

In this section we illustrate the use of the AB- and BA-GMRES methods for CT problems with an unmatched transpose. We start with numerical results related to the eigenvalues of the iterations matrices AB and BA , and then we demonstrate the semi-convergence of the methods. All computations are performed in MATLAB using our own implementations of AB- and BA-GMRES which are available from us, LSQR is from Regularization Tools [14] and LSMR is from MathWorks' File Exchange [7].

Table 6.1: The parameters used to generate the small and large test matrices; the matrix dimensions are $m = N_{\text{ang}}N_{\text{det}}$ and $n = N^2$. We also show the ground truth \bar{x} as an image.

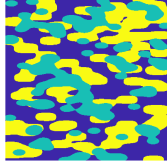
| Parameter | Small matrix | Large matrix | Ground truth |
|--|---|---|---|
| Image size $N \times N$ | 128×128 | 420×420 |  |
| Projection angles | $0^\circ, 1^\circ, 2^\circ, \dots, 179^\circ$ | $0^\circ, 0.3^\circ, 0.6^\circ, \dots, 179.7^\circ$ | |
| No. projection angles N_{ang} | 180 | 600 | |
| No. detector elements N_{det} | 128 | 420 | |
| Matrix size $m \times n$ | $23\,040 \times 16\,384$ | $252\,000 \times 176\,400$ | |
| Sparsity | $\approx 99\%$ | $\approx 99.6\%$ | |

Table 6.2: The relative norm-wise differences between the three test matrices from ASTRA.

| | $\ A_s - A_1\ _F / \ A_s\ _F$ | $\ A_s - A_i\ _F / \ A_s\ _F$ | $\ A_1 - A_i\ _F / \ A_1\ _F$ |
|----------------|-------------------------------|-------------------------------|-------------------------------|
| small matrices | 0.3700 | 0.1402 | 0.2648 |
| large matrices | 0.3747 | 0.1405 | 0.2685 |

6.1 The Test Problems

The matrices A and B used in these experiments are representative for the matrices in many CT software packages and applications. They are generated by means of the CPU version of the software package ASTRA [32]; the matrices in the GPU version are not explicitly available when using this software. Three different discretization models are provided in ASTRA: the line model, the strip model, and the interpolation (or Joseph) model; see [17, Chapter 9] for details. We can then use any of the corresponding matrices A_1 , A_s and A_i to generate unmatched pairs (A, B) . We use a parallel-beam geometry and two different sizes of these matrices corresponding to the parameters listed in Table 6.1, while Table 6.2 lists the relative norm-wise differences between these matrices. The exact solution \bar{x} is generated by means of the function

`phantomgallery('threephases', N)`

from [16], and it is shown in Table 6.1. We add white Gaussian noise e to \bar{b} with two different relative noise level $\|e\|_2 / \|\bar{b}\|_2 = 0.003$ and 0.03 .

6.2 Eigenvalues

As mentioned in the Introduction, the standard SIRT iterative methods will not converge when BA has complex eigenvalues with negative real part. To demonstrate that this is the case for the discretizations used here, Figure 6.1 shows the leftmost and the largest eigenvalues of BA computed by means of MATLAB's `eigs`, for two combinations of the small and large test matrices, namely, $A_1^\top A_s$ and $A_1^\top A_i$. In both cases there are indeed eigenvalues with negative real parts, meaning that the SIRT methods do not converge. Hence, it is natural to use the AB- and BA-GMRES methods for these matrices. The leftmost eigenvalues of the third combination $A_s^\top A_i$ have tiny negative real parts.

6.3 Error Histories

To illustrate the semi-convergence we use both AB-GMRES and BA-GMRES to solve systems with small and large test matrices and with the noise level $\|e\|_2 / \|\bar{b}\|_2 = 0.003$. We tried all six pairs with $B \neq A$, and for comparison we also used LSQR and LSMR (which correspond to the case $B = A^\top$). To check our implementations, we verified numerically that AB- and BA-GMRES with $B = A^\top$ give the same results LSQR and LSMR (we do not show there results

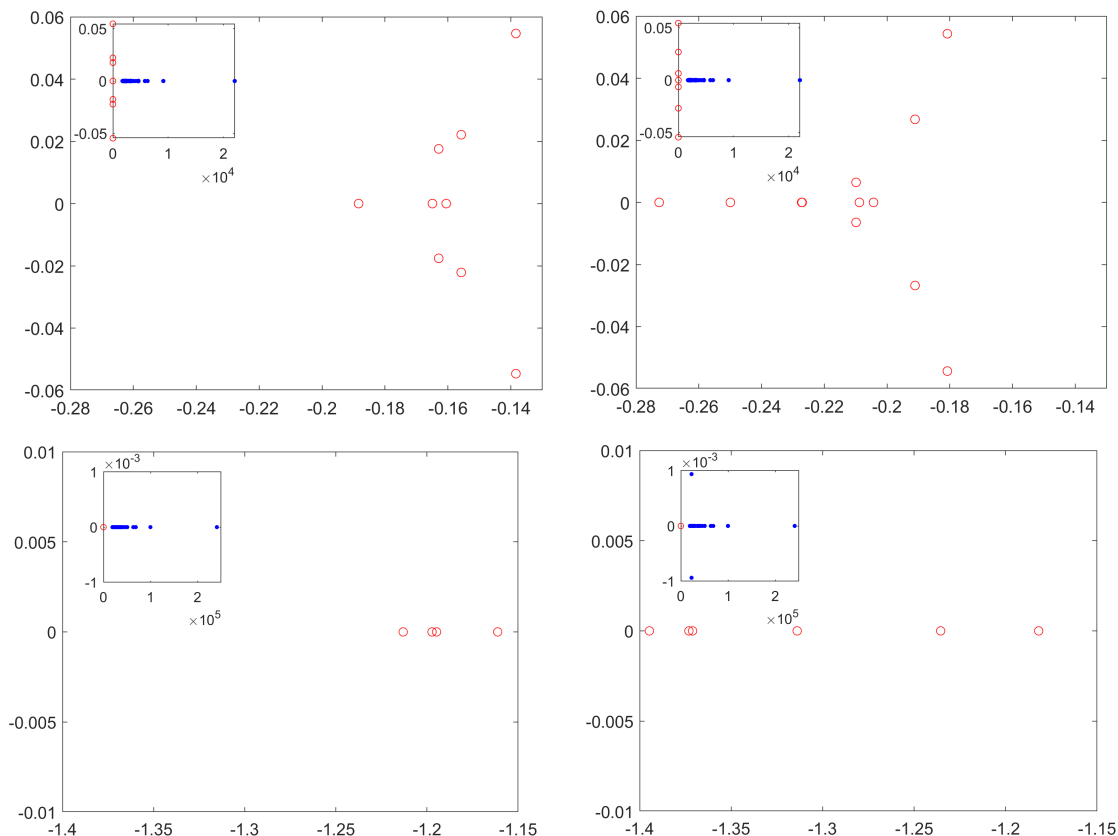


Figure 6.1: Selected eigenvalues of the matrices $A_1^T A_s$ (left) and $A_1^T A_i$ (right), for both the small (top) and large (bottom) test matrices. The red circles show the leftmost eigenvalues all of which have a negative real part. The inset figure shows these eigenvalues together with the 50 largest eigenvalues shown as blue dots.

Table 6.3: For each algorithm and each (A, B) pair, the numbers to the left and right in each block column are results for large and small test matrices, respectively. We list the reconstruction error, the number of iterations (in parenthesis), and on the second line the required storage. Note that the results for LSQR and LSMR are independent of B . See Table 6.2 for the norm-wise differences between the matrices.

| Pair | AB-GMRES | | BA-GMRES | | LSQR | | LSMR | |
|----------------|-------------|-------------|-------------|-------------|-------------|-------------|-------------|-------------|
| (A_s, A_1^T) | 0.1047 (34) | 0.1203 (36) | 0.1039 (38) | 0.1199 (41) | 0.0954 (57) | 0.0996 (62) | 0.0946 (68) | 0.0990 (77) |
| | 8568000 | 829440 | 6703200 | 671744 | | | | |
| (A_s, A_i^T) | 0.0985 (41) | 0.1059 (42) | 0.0978 (47) | 0.1056 (50) | 0.0954 (53) | 0.0996 (61) | 0.0946 (63) | 0.0990 (77) |
| | 10332000 | 967680 | 8290800 | 819200 | | | | |
| (A_1, A_s^T) | 0.0878 (61) | 0.0926 (77) | 0.0871 (74) | 0.0921 (85) | 0.0896 (52) | 0.0879 (64) | 0.0875 (63) | 0.0795 (80) |
| | 15372000 | 1774080 | 13053600 | 1392640 | | | | |
| (A_1, A_i^T) | 0.0899 (50) | 0.0927 (60) | 0.0894 (60) | 0.0922 (69) | 0.0896 (52) | 0.0870 (64) | 0.0875 (63) | 0.0795 (80) |
| | 12600000 | 1382400 | 10584000 | 1130496 | | | | |
| (A_i, A_1^T) | 0.1005 (39) | 0.1112 (42) | 0.0998 (44) | 0.1105 (47) | 0.0935 (53) | 0.0948 (61) | 0.0928 (63) | 0.0940 (77) |
| | 9828000 | 967680 | 7761600 | 770048 | | | | |
| (A_i, A_s^T) | 0.0915 (55) | 0.0930 (68) | 0.0901 (67) | 0.0920 (84) | 0.0935 (53) | 0.0948 (61) | 0.0928 (63) | 0.0940 (77) |
| | 13860000 | 1566720 | 11818800 | 1376256 | | | | |

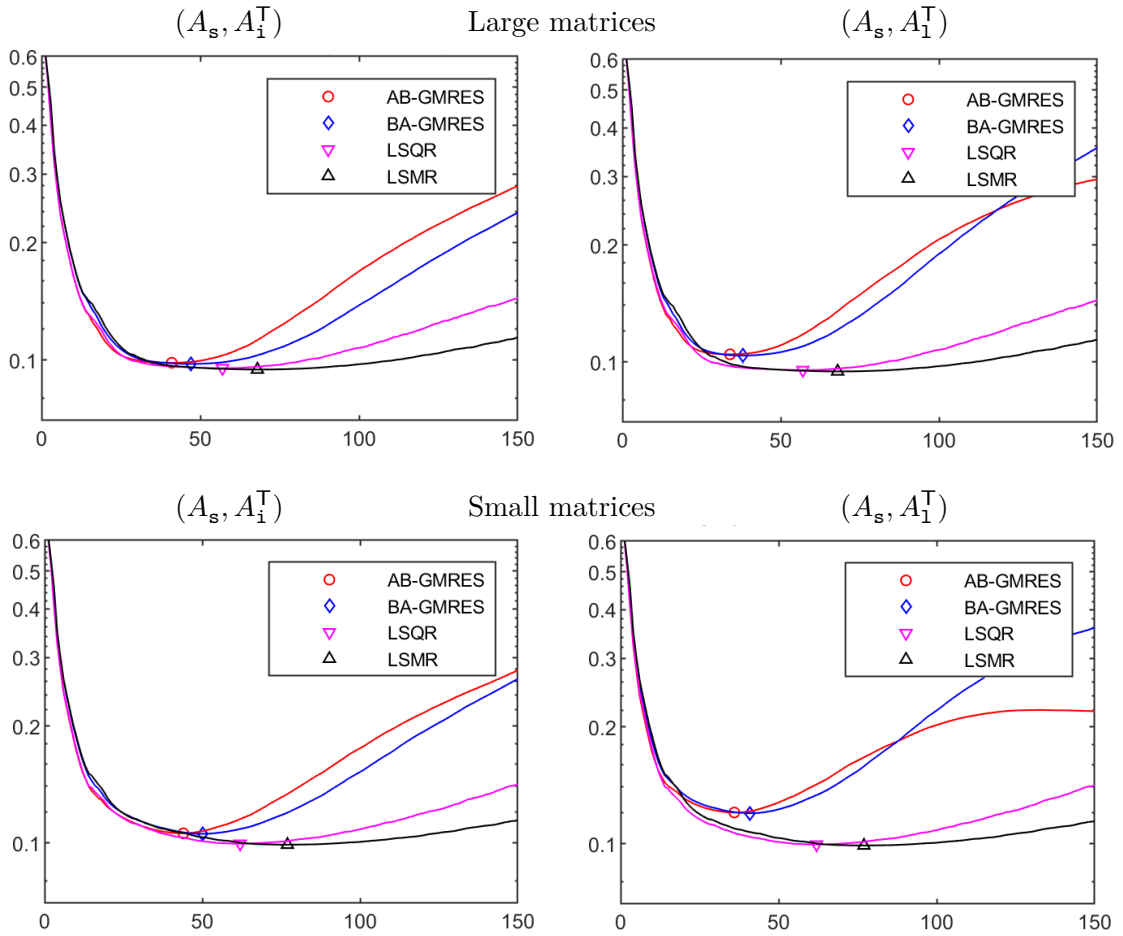


Figure 6.2: Error histories, i.e., plots of the relative reconstruction error $\|\bar{x} - x_k\|_2 / \|\bar{x}\|_2$ versus the number of iterations. The minima are indicated by the markers. We show results for the cases $(A, B) = (A_s, A_1^T)$ in the left plots, and $(A, B) = (A_s, A_1^T)$ in the right plots. The top and bottom plots are for large and small matrices, respectively. The noise level is $\|e\|_2 / \|\bar{b}\|_2 = 0.003$.

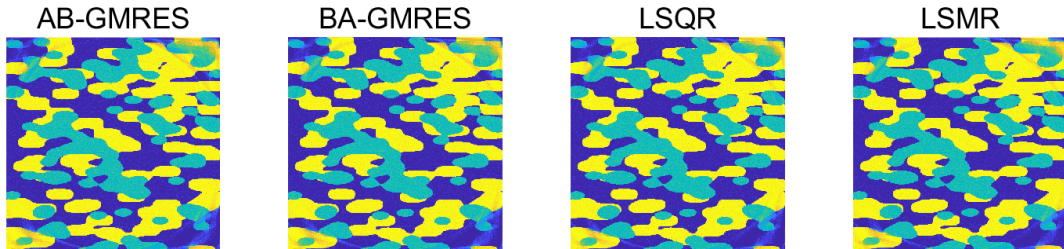


Figure 6.3: Reconstructions for the pair $(A, B) = (A_s, A_1^T)$ at the point of semi-convergence, i.e., the minima of the curves in the top right plot of Figure 6.2. Pixel values below zero and above one are set to zero and one, respectively. The slight artifacts near the corners are always present, and they are due to the scanning geometry with few X-ray penetrating these regions.

here). Figure 6.2 shows the error histories, i.e., the relative reconstruction error $\|\bar{x} - x_k\|_2 / \|\bar{x}\|_2$ versus the number of iterations for the cases $(A, B) = (A_s, A_1^\top)$ and $(A, B) = (A_s, A_1^\top)$. Figure 6.3 shows the reconstructions for the case $(A, B) = (A_s, A_1^\top)$. These results are representative for all six pairs of matrices.

When we refer to the “reconstruction error,” we mean the relative error at the point of semi-convergence (i.e., the minimum of the error histories) indicated by the markers in the plots. The reconstruction errors for all (A, B) pairs are shown in Table 6.3. For each of the six (A, B) pairs we observe the following:

- We obtain almost the same reconstruction error for AB-GMRES and BA-GMRES, cf. block columns 2 and 3.
- We obtain almost the same reconstruction error for LSQR and LSMR, cf. block columns 4 and 5.
- When $A = A_s$ then LSQR and LSMR give slightly smaller reconstruction errors than AB- and BA-GMRES, cf. the top block row as well as Figure 6.2.
- For the other two A matrices, all four methods give almost the same reconstruction errors, cf. the middle and bottom block rows.
- The pairs $(A, B) = (A_1, A_s^\top)$ and $(A, B) = (A_1, A_1^\top)$ give marginally more accurate reconstructions than the other pairs, cf. the middle block row.
- Often, AB-GMRES uses just slightly fewer iterations than BA-GMRES – and occasionally it uses significantly less iterations.
- LSQR always uses less iterations than LSMR.

We also carried out experiments with under-determined problems (which are not documented here). The conclusions remain the same.

Table 6.3 also lists the required amount of storage for the orthogonal q_k -vectors which are of length m and n for AB-GMRES and BA-GMRES, respectively. For the overdetermined systems used here with $m \approx 1.4n$, in spite of BA-GMRES consistently using more iterations than AB-GMRES, BA-GMRES requires less storage due to the shorter q_k -vectors. For underdetermined systems (not reported here), AB-GMRES has the advantage of less iterations and shorter q_k -vectors, cf. [19, p. 2408].

We emphasize that the choice of A and B is dictated by the available software, and therefore one may not always have a choice of the implementation used in A and B . Moreover, the above results are for matrices used in the ASTRA software (which allows easy access to the matrices); other packages may use different discretization methods. We also stress that in these experiments we perform inverse crime, meaning that the noise-free data is generated as $\bar{b} = A \bar{x}$; hence the data is different for the three choices of A meaning that we do not solve precisely the same problem for each choice of A . Therefore, the above results provide important insight about the influence of $B \neq A^\top$, but they do not determine what is the best choice of A and B for a CT problem with real data and no inverse crime.

6.4 Stopping Rules

Here we demonstrate the use of two stopping rules that seek to terminate the iterations at the point of semi-convergence.

- The **discrepancy principle (DP)** [26] terminates the iterations as soon as the residual norm is smaller than the noise level:

$$k_{\text{DP}} = \text{the smallest } k \text{ for which } \|b - Ax_k\|_2 \leq \tau \|e\|_2 \quad .$$

Here, $\tau \geq 1$ is a “safety factor” that can be used when we have only a rough estimate of $\|e\|_2$. We use $\tau = 1$ and the exact value of $\|e\|_2$.

- The **NCP criterion** uses the normalized cumulative periodogram to perform a spectral analysis of the residual vector $b - Ax_k$, in order to identify when the residual is as close to being white noise as possible, which indicates that all available information has been extracted from the noisy data. See [16, Section 2.3.3] and [18, SectionII.D] for details; MATLAB code is available from us.

We apply these stopping rules to the same pairs $(A, B) = (A_s, A_1^T)$ and $(A, B) = (A_s, A_1^T)$ as in Figure 6.2, with the same noise level $\|e\|_2/\|\bar{b}\|_2 = 0.003$, and the results are shown in Figure 6.4. We obtain similar results for the other (A, B) pairs and hence they are not shown here. We make the following observations:

- Both DP and NCP stop the iterations before the minimum is reached. This is better than stopping too late, in which case we would include undesired noise in the solution.
- Both DP and NCP stop the iterations when the error history starts to level off; the minimum of the error history is quite flat so this is acceptable.
- For unknown reasons, NCP always stops the iterations a bit earlier than DP.

We conclude that both stopping rules work well for this problem. The DP stopping rule requires a good estimate of the noise level; if this is not available (as is typical in CT problems) then the performance of NCP is only slightly inferior to DP.

6.5 SVD Analysis of Semi-Convergence

More detailed insight into the semi-convergence can be obtained by means of the SVD of A , and we present results for the small test matrices $(A, B) = (A_s, A_1^T)$ (for the large matrices we were not able to compute enough SVD components with MATLAB’s `svds`). Figure 6.5 shows the singular values together with the right-hand side’s SVD coefficients $|u_i^T \bar{b}|$ for the exact data and $|u_i^T b|$ for noisy data with noise level $\|e\|_2/\|\bar{b}\|_2 = 0.003$. The behavior of the singular values is typical for discretizations of CT problems – all the large ones decay like those of the underlying Radon transform while the smaller ones decay faster due to discretization effects. We see that the exact data satisfy the DPC, i.e., they decay at least as fast as the singular values. We also clearly see the “noise floors” in the right plots of $|u_i^T b|$ around 0.5.

Figure 6.6 shows, for selected values of k , the SVD coefficients $|v_i^T \bar{x}|$ (red) for the exact solution together with the SVD coefficients $|v_i^T x_k|$ (blue) for selected the iterates x_k with noisy data with noise level $\|e\|_2/\|\bar{b}\|_2 = 0.003$. Again we use the small test matrices. For all four methods, as k increases we capture an increasing amount of SVD components, and at $k = 30$ we have already computed good approximations of the first 10 000 exact SVD components. As we perform further iterations we start to capture unwanted SVD components associated with small singular values; these components are influenced by noise causing the blue dots to form a “bump” that lies distinctly above the red dots. This is particularly pronounced for AB- and BA-GMRES after $k = 100$ iterations. These “bumps” are obviously not present for noise-free data (not shown here).

In Figure 6.6 we also observe a distinctly different behavior of LSQR and LSMR versus AB- and BA-GMRES. As discussed, e.g., in [13, Section 6.3.2], LSQR is a spectral filtering method that produces filtered SVD solution conforming with (4.2), and the same is true for LSMR which uses the same Krylov subspace. For the smaller singular values the filter factors behave as $\phi_i^{(k)} = O(\sigma_i^2)$ meaning that they decay fast to zero, causing the blue dots to “drop off” very fast – for example, at $k = 30$ iterations the LSQR and LSMR iterates contain practically no SVD coefficients with index $i > 12\,000$. As we perform more iterations, eventually a small

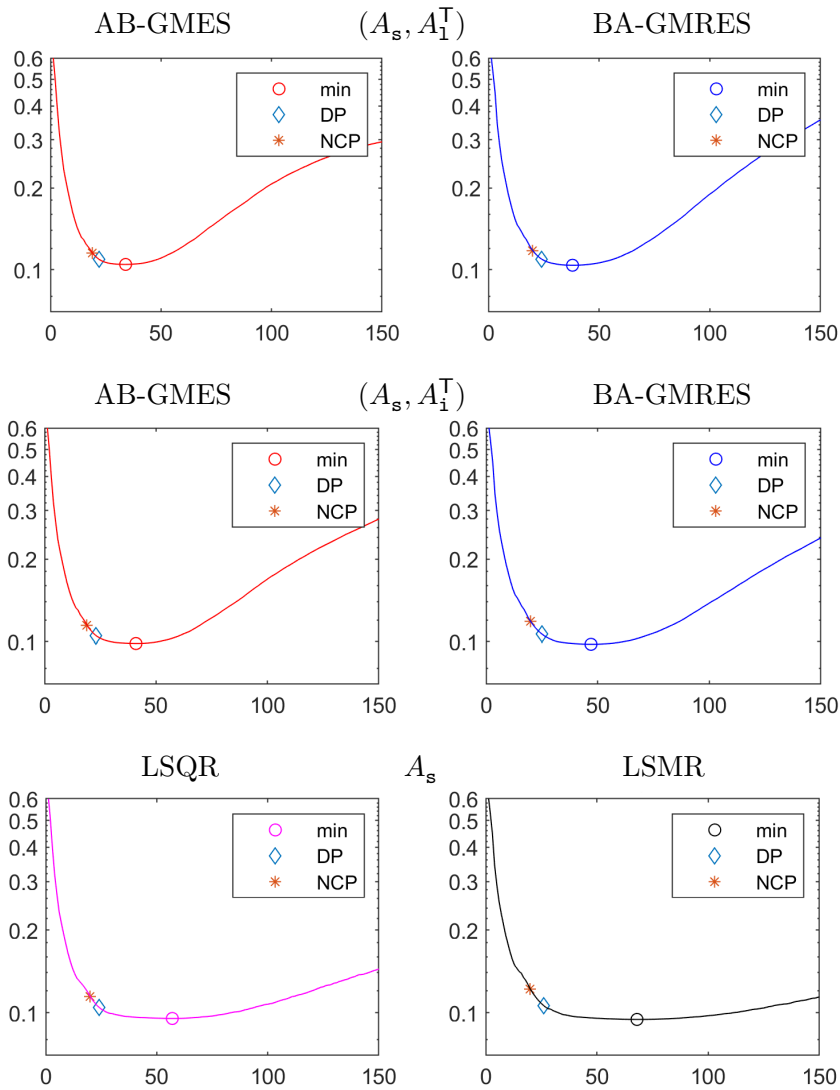


Figure 6.4: We show the error histories $\|\bar{x} - x_k\|_2 / \|\bar{x}\|_2$ versus the number of iterations. The markers indicate the minimum as well as the error at the number of iterations k_{DP} and k_{NCP} found by the discrepancy principle and the NCP criterion, respectively. We show AB- and BA-GMRES results for the cases $(A, B) = (A_s, A_1^T)$ and $(A, B) = (A_s, A_i^T)$, as well as LSQR and LSMR results for A_s , similarly to Figure 6.2 and with the same noise level $\|e\|_2 / \|\bar{b}\|_2 = 0.003$.

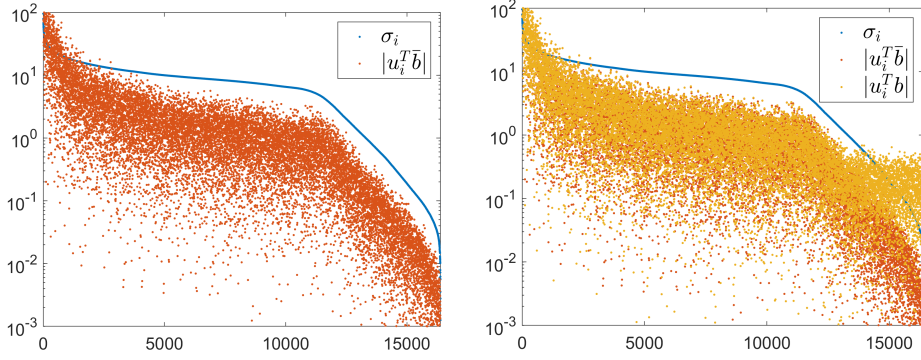


Figure 6.5: Plots of the singular values σ_i (blue dots) and the right-hand side's SVD coefficients $|u_i^T \bar{b}|$ for the exact data (red dots) and $|u_i^T b|$ for noisy data (brown dots). The left plot shows only σ_i and $|u_i^T \bar{b}|$ while the right plot shows all three quantities for the noise level $\|e\|_2/\|\bar{b}\|_2 = 0.003$.

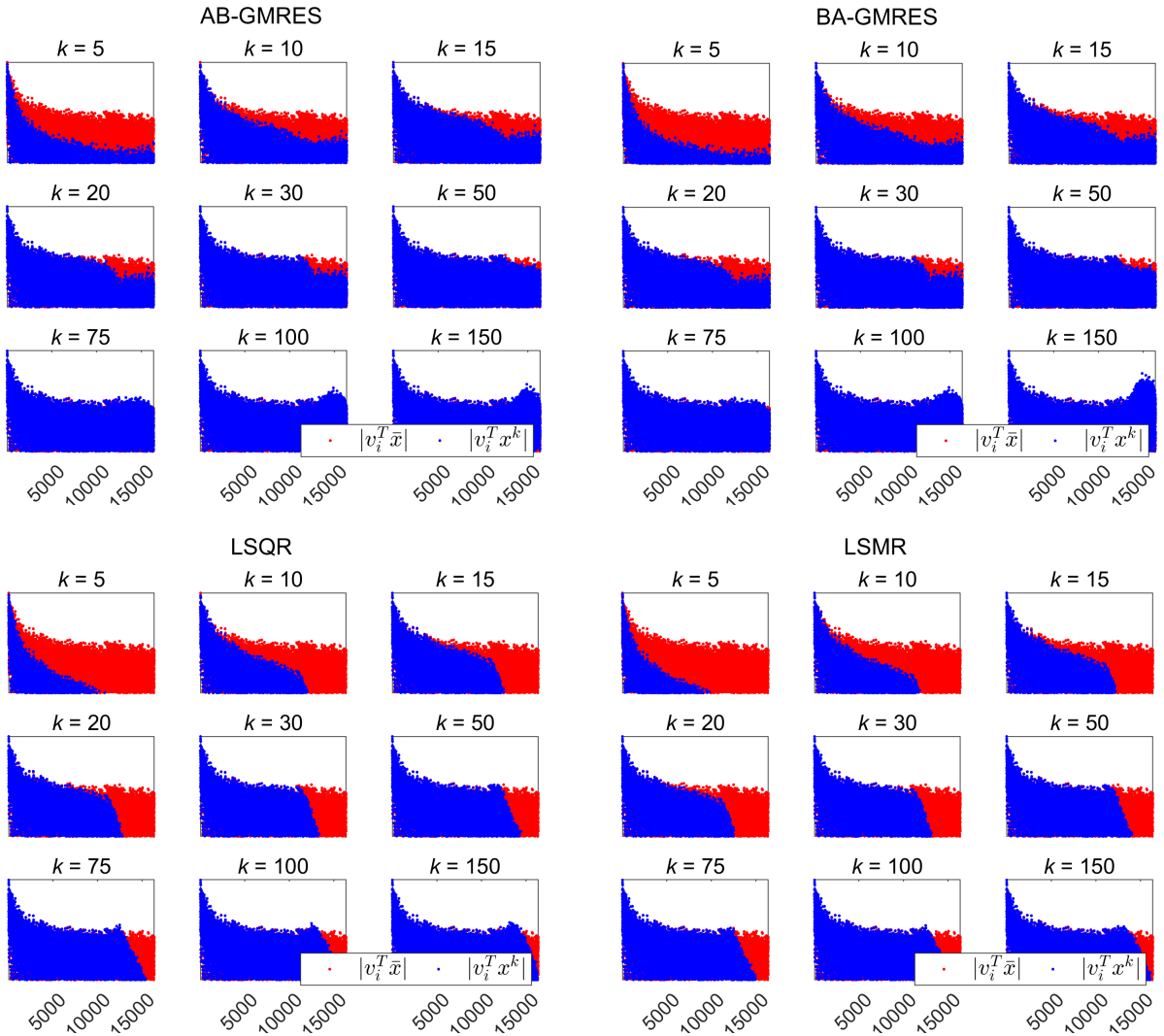


Figure 6.6: SVD analysis of the iterates x_k for selected values of the iteration number k , for the low noise level $\|e\|_2/\|\bar{b}\|_2 = 0.003$. Red dots: SVD coefficients $|v_i^T \bar{x}|$ for the exact solution. Blue dots: SVD coefficients $|v_i^T x_k|$.

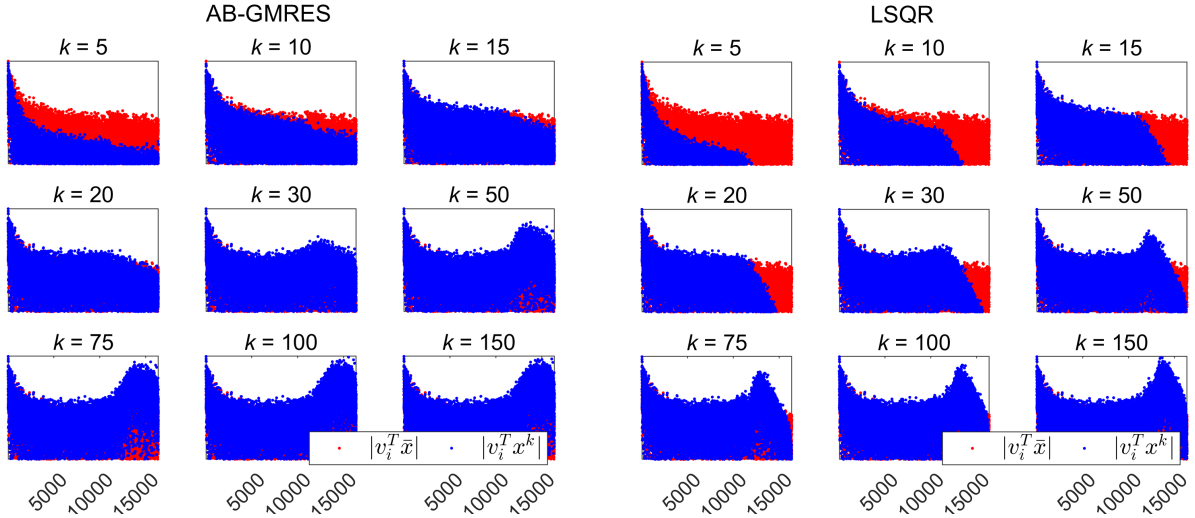


Figure 6.7: SVD analysis similar to Figure 6.6 for the larger noise level $\|e\|_2/\|\bar{b}\|_2 = 0.03$.

“bump” starts to appear for large indices $i > 10000$; it is clearly visible at $k = 150$ but it is much less pronounced than for AB- and BA-GMRES.

AB- and BA-GMRES, on the other hand, are not spectral filtering methods of the form (4.2), due to the underlying Krylov subspace $\mathcal{K}_k(BA, Bb)$, and SVD coefficients for all $i = 1, \dots, n$ are present in all iterations (some larger and some smaller). This causes the noise to enter the iterates faster, and hence the reconstruction error (at the point of semi-convergence) tends to be larger for AB- and BA-GMRES.

Figure 6.7 shows the SVD coefficients for AB-GMRES and LSQR, similar to Figure 6.6, for the larger noise level $\|e\|_2/\|\bar{b}\|_2 = 0.03$. The overall behavior is similar to that in the previous figure, except that the undesired “bump” now appears after only $k = 30$ iterations.

6.6 Varying the Back Projector’s Unmatchedness

We conclude with numerical experiments where we study the influence of the back projector’s *unmatchedness*, as measured by $\|B - A^\top\|_F/\|A\|_F$. So far we have considered matrices A and B generated by the ASTRA software package, which are representative examples of the matrices that we encounter with CT reconstruction software. The disadvantage is that we cannot control ourselves how much B deviates from A^\top . For this reason we introduce a new set of back projection matrices B_τ defined by neglecting elements of A^\top according to a threshold τ . Specifically, if $(\cdot)_{ij}$ denotes matrix elements then we define

$$(B_\tau)_{ij} = \begin{cases} (A)_{ji} & \text{if } (A)_{ji} \geq \tau \max_{ij}(A)_{ij} \\ 0 & \text{else.} \end{cases} \quad (6.1)$$

We do not need absolute values since all matrix elements are nonnegative. When $\tau = 0$ then $B = A^\top$ is perfectly matched, and the larger the τ the more unmatched the B . We emphasize that these unmatched matrices do not represent actual implementations of back projections in CT software packages.

We focus on the large 252000×176400 test matrix A_s generated with the strip model. Figure 6.8 shows relative error histories $\|\bar{x} - x_k\|_2/\|\bar{x}\|_2$ for both AB-GMRES and BA-GMRES, for difference choices of τ , see Table 6.4, and with a noise-free as well as a noisy right-hand side with $\|e\|_2/\|\bar{b}\|_2 = 0.003$. We make the following observations:

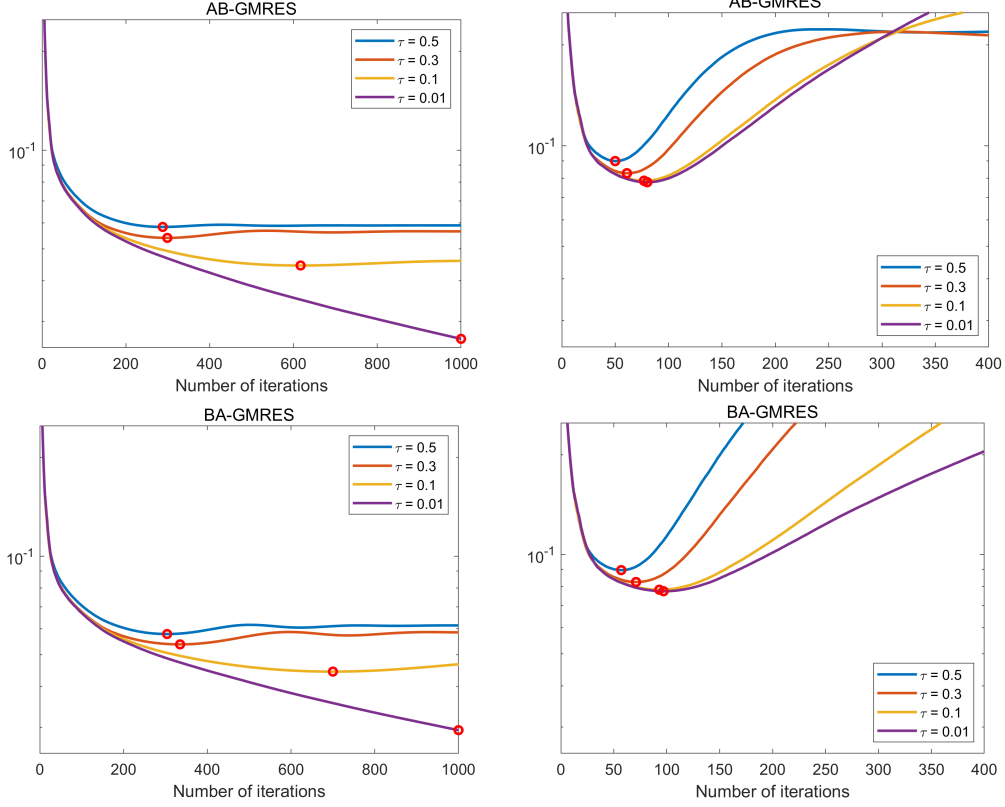


Figure 6.8: Error histories for four pairs (A_s, B_τ) with four different values of τ . The top and bottom plots are for the AB-GMRES and BA-GMRES methods, respectively. The left plots use a noise-free right-hand side \bar{b} and the right plots are for noisy data $b = \bar{b} + e$ with $\|e\|_2 / \|\bar{b}\|_2 = 0.003$. The minima are marked with red circles.

Table 6.4: Corresponding values of τ , the measure of unmatchedness.

| τ | 0.01 | 0.1 | 0.3 | 0.5 | comment |
|------------------------------------|--------|--------|--------|--------|----------------|
| $\ B_\tau - A_s^T\ _F / \ A_s\ _F$ | 0.0021 | 0.0386 | 0.1640 | 0.3366 | small matrices |
| | 0.0021 | 0.0387 | 0.1650 | 0.3397 | large matrices |

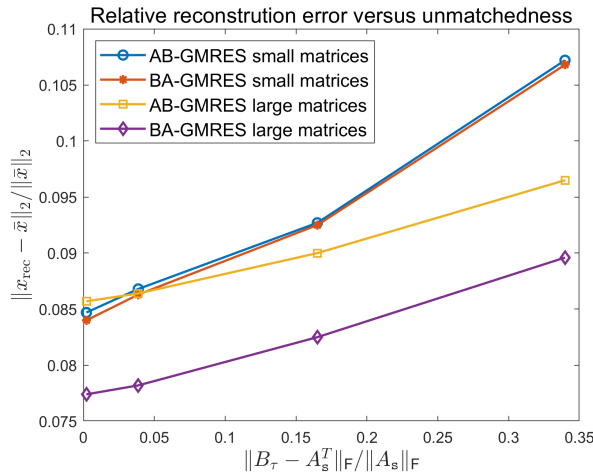


Figure 6.9: The relative reconstruction error versus the unmatchedness for the pair (A_s, B_τ) .

1. Both methods converge to the solution x_τ^{UNE} to the unmatched normal equations (1.2). When $B_\tau = A_s^\top$ and $e = 0$ (no noise) then x_τ^{UNE} equals the ground truth \bar{x} , and they differ otherwise. The difference $x_\tau^{\text{UNE}} - \bar{x}$ increases as τ increases and as $\|e\|_2$ increases.
2. The reconstruction error consists of two components: the iteration error $x_\tau^{\text{UNE}} - x_k$ and the error $\bar{x} - x_\tau^{\text{UNE}}$ caused by $B_\tau \neq A^\top$. For small τ the first component dominates, while both components may contribute for large τ .
3. For noise-free data the minimum error is entirely determined by the norm $\|B_\tau - A_s^\top\|_F$.
4. For noisy data, where we have semi-convergence, for all four values of τ the minimum is mainly determined by the error e .
5. For $\tau = 0.5$ we have $\|B_\tau - A_s^\top\|_F/\|A_s\|_F = 0.34$ and the error histories resemble those for the pair (A_s, A_1^\top) in Figure 6.2, for which $\|A_s - A_1^\top\|_F/\|A_s\|_F = 0.37$ (almost the same amount of unmatchedness).
6. For $\tau = 0.01$ we have that B_τ is almost a matched transpose, and the error histories resemble those for LSQR and LSMR in Figure 6.2.

These results confirm our theory, namely, that the behavior of AB-GMRES and BA-GMRES resembles that of LSQR and LSMR, respectively, when $\tau \rightarrow 0$. Moreover, for large τ the behavior of AB- and BA-GMRES with $B = B_\tau$ resembles that with the ASTRA matrices.

Figure 6.9 shows the relative reconstruction error $\|x_{\text{rec}} - \bar{x}\|_2/\|\bar{x}\|_2$ versus the unmatchedness, where x_{rec} is the iteration vector at the minimum (the point of semi-convergence). We observe a linear dependence between the two quantities.

Similar to the SVD analysis in the previous subsection, we can use the SVD of A_s to analyze the semi-convergence of AB- and BA-GMRES applied to (A_s, B_τ) for $\tau = 0.01, 0.1, 0.3$ and 0.5 . For this analysis we use the small test matrix A_s (because we need to compute the full SVD) and Table 6.4 shows the corresponding $\|B_\tau - A_s^\top\|_F/\|A_s\|_F$. The relative noise level is $\|e\|_2/\|\bar{b}\|_2 = 0.003$. The results are shown in Figure 6.10.

1. This behavior and the plots are practically identical for AB-GMRES and BA-GMRES.
2. For $\tau = 0.01$ the behavior is, as expected, almost similar to that for LSQR/LSMR shown in Figure 6.6 (which corresponds to the case $\tau = 0$). Specifically, during the first iterations we do not include undesired noisy SVD components corresponding to the small singular values.
3. As τ increases the behavior starts to resemble the case (A_s, A_1^\top) shown in Figure 6.6, where we – even during the first iterations – include more undesired SVD components as compared to LSQR/LSMR.

Again these results confirm our theory about the connection between the unmatchedness $\|A_1^\top - A_s^\top\|_F/\|A_s\|_F$ and the behavior of the iterative methods.

7 Conclusion

The AB- and BA-GMRES algorithms can be considered as preconditioned versions of the well-known GMRES algorithm, and we discuss how to use these algorithms for solving large-scale X-ray CT problems with an unmatched projector. We also study the behavior of AB- and BA-GMRES as the back projector approaches a matched one. Numerical experiments, including numerical SVD analysis, provide the insight that AB- and BA-GMRES exhibit semi-convergence and thus they behave as regularizing iterative methods where the number of iterations is the regularization parameter (similar to the behavior as LSQR/LSMR). Our numerical experiments

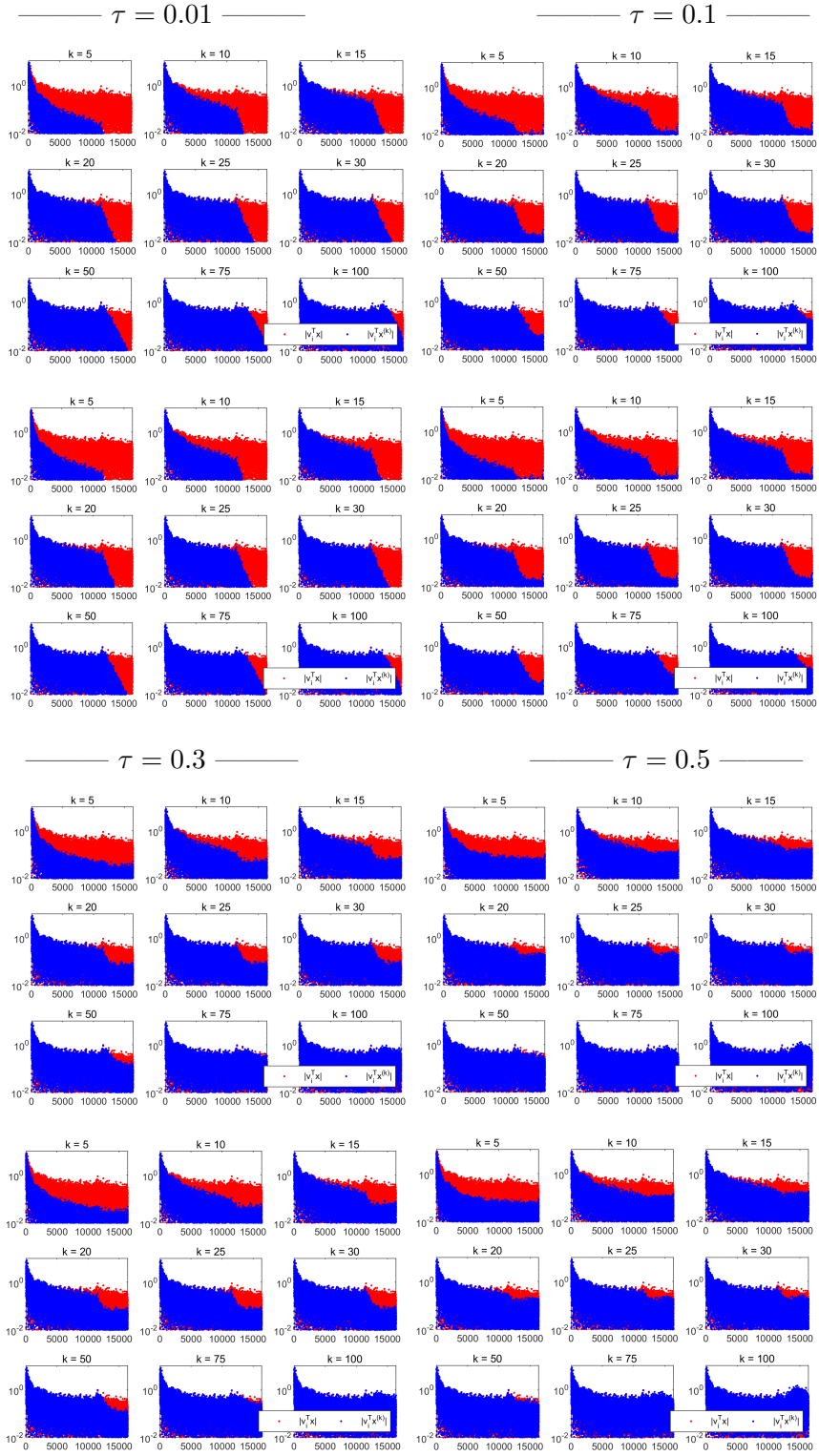


Figure 6.10: SVD analysis of the iterates of AB-GMRES (top) and BA-GMRES (bottom) for the unmatched transpose B_τ generated according to (6.1), similar to Figures 6.6 and 6.7. The noise level is $\|e\|_2/\|\bar{b}\|_2 = 0.003$.

also demonstrate that the discrepancy principle and the NCP-criterion work well as stopping rules. We recommend software developers to consider AB- and BA-GMRES for the solution of large-scale CT reconstruction problems.

A Proof of Theorem 3.1

We introduce notation required for the assertions below. Denote the rank of A by r . Let $U = [U_1, U_2] \in \mathbb{R}^{m \times m}$ be an orthogonal matrix with $\mathcal{R}(U_1) = \mathcal{R}(A)$ and $\mathcal{R}(U_2) = \mathcal{R}(A)^\perp$, where $U_1 \in \mathbb{R}^{m \times r}$ and $U_2 \in \mathbb{R}^{m \times (m-r)}$. Let $V = [V_1, V_2] \in \mathbb{R}^{n \times n}$ be an orthogonal matrix with $\mathcal{R}(V_1) = \mathcal{N}(A)^\perp$ and $\mathcal{R}(V_2) = \mathcal{N}(A)$, where $V_1 \in \mathbb{R}^{n \times r}$ and $V_2 \in \mathbb{R}^{n \times (n-r)}$. Then, we transform the unmatched normal equations via U and V into

$$V^\top \tilde{B} \tilde{A} U U^\top (x_{\min} + \delta x_{\min}) = V^\top \tilde{B} U U^\top b,$$

in which

$$U^\top A V = \begin{bmatrix} A_{11} & \mathbf{O} \\ \mathbf{O} & \mathbf{O} \end{bmatrix}, \quad U^\top E_k V = \begin{bmatrix} E_{11}^{(k)} & E_{12}^{(k)} \\ E_{21}^{(k)} & E_{22}^{(k)} \end{bmatrix}$$

for $k = 1, 2$, where $A_{11} = U_1^\top A V_1$, $E_{ij}^{(k)} = U_i^\top E_k V_j$ for $i, j = 1, 2$. Hereafter, we neglect higher-order terms to derive a first-order perturbation bound for δx_{\min} . Thus, we obtain a first-order approximation of the transformed coefficient matrix of (3.2)

$$V^\top \tilde{B}^\top U U^\top \tilde{A} V = \begin{bmatrix} G & A_{11}^\top E_{12}^{(1)} \\ (E_{12}^{(2)})^\top A_{11} & \mathbf{O} \end{bmatrix}, \quad (\text{A.1})$$

where $G = A_{11}^\top A_{11} + F$ with $F = A_{11}^\top E_{11}^{(1)} + (E_{11}^{(2)})^\top A_{11}$, and the right-hand side vector of (3.2) together with V^\top

$$V^\top \tilde{B} U U^\top b = \begin{bmatrix} A_{11}^\top \bar{b}_1 + A_{11}^\top \delta b_1 + (E_{11}^{(2)})^\top \bar{b}_1 + (E_{21}^{(2)})^\top \bar{b}_2 \\ (E_{12}^{(2)})^\top \bar{b}_1 + (E_{22}^{(2)})^\top \bar{b}_2 \end{bmatrix},$$

where $b_i = U_i^\top b$, $i = 1, 2$, and $\delta b_1 = U_1^\top \delta b$.

Lemma A1. *Assume that \tilde{A} and \tilde{B} are both acute perturbations of A . The first-order bound of the relative error norm is given by*

$$\frac{\|\delta x_{\min}\|_2}{\|x_{\min}\|_2} \leq \kappa_2(A) \left\{ \sigma_r^{-1} \left[\left(\|E_{11}^{(1)}\|_2 + \|E_{12}^{(1)}\|_2 \right) \frac{\|\bar{b}_1\|_2}{\|\bar{b}\|_2} + \frac{\|(E_{21}^{(2)})^\top \bar{b}_2\|_2}{\|\bar{b}\|_2} \right] + \frac{\|\delta b_1\|_2}{\|\bar{b}\|_2} \right\},$$

where $\kappa_2(A) = \|A\|_2 \|A^\dagger\|_2$ is the condition number of A and σ_r is the nonzero smallest singular value of A .

Proof of Lemma A1. The assumptions imply that there is no vector in $\mathcal{R}(A)$ that is orthogonal to $\mathcal{R}(\tilde{A})$ and $\mathcal{R}(\tilde{B})$, $\text{rank}(A) = \text{rank}(\tilde{A}) = \text{rank}(\tilde{B})$ [31, Theorem 3.1], and A_{11} is nonsingular [31, Theorem 3.3]. We use the formula in [20] for the pseudoinverse of a block two-by-two matrix to (A.1). Let $C = V^\top \tilde{B}^\top U U^\top \tilde{A} V$. Then,

$$C^\dagger = \begin{bmatrix} (G^\dagger)^\top & (G^\top G)^\dagger A_{11}^\top E_{12}^{(2)} \\ (E_{12}^{(1)})^\top A_{11} (G^\dagger)^\top G^\dagger & \mathbf{O} \end{bmatrix}.$$

Therefore, the minimum-norm solution together with V is given by

$$V^\top (x_{\min} + \delta x_{\min}) = C^\dagger V^\top \tilde{B} U U^\top b$$

$$= \begin{bmatrix} (G^\dagger)^\top \left[A_{11}^\top (\bar{b}_1 + \delta b_1) + (E_{11}^{(2)})^\top \bar{b}_1 + (E_{21}^{(2)})^\top \bar{b}_2 \right] \\ (E_{12}^{(1)})^\top A_{11} (G^\dagger)^\top G^\dagger A_{11}^\top \bar{b}_1 \end{bmatrix}.$$

Applying the formula in [21] for the pseudoinverse of the sum of two matrices to $G^\dagger = (A_{11}^\top A_{11} + F)^\dagger$, we obtain $G^\dagger = (A_{11}^\top A_{11})^{-1} - L$, where $L = (A_{11}^\top A_{11})^{-1} F (A_{11}^\top A_{11})^{-1}$. Therefore, we have

$$V^\top (x_{\min} + \delta x_{\min}) = \begin{bmatrix} A_{11}^{-1} (\bar{b}_1 + \delta b_1) + (A_{11}^\top A_{11})^{-1} \left[(E_{11}^{(2)})^\top \bar{b}_1 + (E_{21}^{(2)})^\top \bar{b}_2 \right] - L^\top A_{11}^\top \bar{b}_1 \\ (E_{12}^{(1)})^\top (A_{11}^\top A_{11})^{-1} \bar{b}_1 \end{bmatrix}.$$

As

$$V^\top x_{\min} = \begin{bmatrix} A_{11}^{-1} \bar{b}_1 \\ \mathbf{0} \end{bmatrix},$$

we have

$$V^\top \delta x_{\min} = \begin{bmatrix} -A_{11}^{-1} E_{11}^{(1)} A_{11}^{-1} \bar{b}_1 + A_{11}^{-1} \delta b_1 + (A_{11}^\top A_{11})^{-1} (E_{21}^{(2)})^\top \bar{b}_2 \\ (E_{12}^{(1)})^\top (A_{11}^\top A_{11})^{-1} \bar{b}_1 \end{bmatrix}.$$

The proof is completed by bounding $\|V^\top \delta x_{\min}\|_2 = \|\delta x_{\min}\|_2$, together with $\|x_{\min}\|_2 \geq \|A\|_2^{-1} \|\bar{b}\|_2$. \square

Proof of Theorem 3.1. It follows from Lemma A1 that we have

$$\begin{aligned} \|\delta x_{\min}\|_2 &\leq \sigma_r^{-2} \left[\left(\|P_{\mathcal{R}(A)} E_1 P_{\mathcal{R}(A)^\top}\|_2 + \|P_{\mathcal{R}(A)} E_1 P_{\mathcal{N}(A)}\|_2 \right) \|P_{\mathcal{R}(A)} \bar{b}\|_2 + \|P_{\mathcal{R}(A)^\top} E_2 P_{\mathcal{R}(A)^\perp} \bar{b}\|_2 \right] \\ &\quad + \sigma_r^{-1} \|P_{\mathcal{R}(A)} \delta b\|_2 \\ &\leq \sigma_r^{-2} \left(2 \|E_1\|_2 \|\bar{b}\|_{\mathcal{R}(A)} + \|E_2\|_2 \|\bar{b}\|_{\mathcal{R}(A)^\perp} \right) + \sigma_r^{-1} \|\delta b\|_{\mathcal{R}(A)}. \end{aligned}$$

\square

An alternative proof of Theorem 3.1 can be given by directly applying the formula in [21] to the sum of $A^\top A$ and $A^\top E_1 + E_2 A$.

Alternative proof of Theorem 3.1. We use the formula in [21] for the pseudoinverse of the sum of two matrices $(A^\top A + E)^\dagger$, where $E = A^\top E_1 + E_2 A$. For convenience, let $M = A^\top A E + E^\top A^\top A$ and

$$T_n = (t_{ij}) \in \mathbb{R}^{n \times n}, \quad t_{ij} = \begin{cases} 1, & j = n - i + 1, \\ 0, & \text{otherwise.} \end{cases}$$

Note $T_n^2 = \mathbf{I}$. Then,

$$\begin{aligned} &(A^\top A + E)^\dagger \\ &= T_n \left(T_n \left[(A^\top A)^2 \right]^\dagger T_n \left\{ T_n - T_n M \left[(A^\top A)^2 \right]^\dagger \right\} + T_n P_{\mathcal{N}(A)} M \left[(A^\top A)^4 \right]^\dagger \right) (A^\top A + E^\top) \\ &= \left\{ \mathbf{I} - \left[(A^\top A)^2 \right]^\dagger M + P_{\mathcal{N}(A)} M \left[(A^\top A)^2 \right]^\dagger \right\} \left[(A^\top A)^2 \right]^\dagger (A^\top A + E^\top) \\ &= \left\{ \mathbf{I} - \left[(A^\top A)^2 \right]^\dagger M + P_{\mathcal{N}(A)} M \left[(A^\top A)^2 \right]^\dagger \right\} (A^\top A)^\dagger + \left[(A^\top A)^2 \right]^\dagger E^\top \\ &= (A^\top A)^\dagger - \left[(A^\top A)^2 \right]^\dagger (A^\top A E + E^\top A^\top A) (A^\top A)^\dagger + P_{\mathcal{N}(A)} (A^\top A E + E^\top A^\top A) \left[(A^\top A)^3 \right]^\dagger \end{aligned}$$

$$\begin{aligned}
& + \left[(A^\top A)^2 \right]^\dagger E^\top \\
& = (A^\top A)^\dagger - (A^\top A)^\dagger E (A^\top A)^\dagger - \left[(A^\top A)^2 \right]^\dagger E^\top P_{\mathcal{R}(A^\top)} + P_{\mathcal{N}(A)} E^\top \left[(A^\top A)^2 \right]^\dagger \\
& \quad + \left[(A^\top A)^2 \right]^\dagger E_1^\top A + (AA^\top A)^\dagger E_2^\top \\
& = (A^\top A)^\dagger - A^\dagger E_1 (A^\top A)^\dagger - (A^\top A)^\dagger E_2 (A^\dagger)^\top - \left[(A^\top A)^2 \right]^\dagger E_1^\top A - (AA^\top A)^\dagger E_2^\top P_{\mathcal{R}(A^\top)} \\
& \quad + P_{\mathcal{N}(A)} E_1^\top (A^\top AA^\top)^\dagger + \left[(A^\top A)^2 \right]^\dagger E_1^\top A + (AA^\top A)^\dagger E_2^\top \\
& = (A^\top A)^\dagger - A^\dagger E_1 (A^\top A)^\dagger - (A^\top A)^\dagger E_2 (A^\dagger)^\top - (AA^\top A)^\dagger E_2^\top P_{\mathcal{R}(A^\top)} + P_{\mathcal{N}(A)} E_1^\top (A^\top AA^\top)^\dagger \\
& \quad + (AA^\top A)^\dagger E_2^\top.
\end{aligned}$$

Applying this matrix to \tilde{B} , we have

$$(A^\top A + E)^\dagger \tilde{B} = A^\dagger - A^\dagger E_1 A^\dagger - (A^\top A)^\dagger E_2^\top P_{\mathcal{R}(A)} + P_{\mathcal{N}(A)} E_1^\top (AA^\top)^\dagger + (A^\top A)^\dagger E_2^\top.$$

Hence, the minimum-norm solution of (3.2) is given by

$$\begin{aligned}
& (\tilde{B}\tilde{A})^\dagger \tilde{B}b \\
& = (A^\top A + E)^\dagger (A^\top + E_2^\top) (\bar{b} + \delta b) \\
& = \left[A^\dagger - A^\dagger E_1 A^\dagger - (A^\top A)^\dagger E_2^\top P_{\mathcal{R}(A)} + P_{\mathcal{N}(A)} E_1^\top (AA^\top)^\dagger + (A^\top A)^\dagger E_2^\top \right] (\bar{b}|_{\mathcal{R}(A)} + \bar{b}|_{\mathcal{R}(A)^\perp}) \\
& \quad + A^\dagger (\delta b|_{\mathcal{R}(A)} + \delta b|_{\mathcal{R}(A)^\perp}) \\
& = \left[A^\dagger - A^\dagger E_1 A^\dagger + P_{\mathcal{N}(A)} E_1^\top (AA^\top)^\dagger \right] \bar{b}|_{\mathcal{R}(A)} + (A^\top A)^\dagger E_2^\top \bar{b}|_{\mathcal{R}(A)^\perp} + A^\dagger \delta b|_{\mathcal{R}(A)}.
\end{aligned}$$

Therefore, the error is given by

$$\begin{aligned}
\delta x_{\min} & = (\tilde{B}\tilde{A})^\dagger \tilde{B}b - A^\dagger \bar{b} \\
& = \left[-A^\dagger E_1 A^\dagger + P_{\mathcal{N}(A)} E_1^\top (AA^\top)^\dagger \right] \bar{b}|_{\mathcal{R}(A)} + (A^\top A)^\dagger E_2^\top \bar{b}|_{\mathcal{R}(A)^\perp} + A^\dagger \delta b|_{\mathcal{R}(A)}.
\end{aligned}$$

The proof can be completed by bounding $\|\delta x_{\min}\|_2$. □

References

- [1] D. CALVETTI, B. LEWIS, AND L. REICHEL, *On the regularizing properties of the GMRES method*, Numerische Mathematik, 91 (2002), pp. 605–625.
- [2] E. COUZENOIX, J.-C. PESQUET, C. RIDDELL, M. SAVANIER, AND Y. TROUSSET, *Convergence of proximal gradient algorithm in the presence of adjoint mismatch*, Inverse Problems, 37 (2021), p. 065009.
- [3] Y. DONG, P. C. HANSEN, M. E. HOCHSTENBACH, AND N. A. B. RIIS, *Fixing nonconvergence of algebraic iterative reconstruction with an unmatched backprojector*, SIAM J. Sci. Comput., 41 (2019), pp. A1822–A1839.
- [4] Y.-S. DU, K. HAYAMI, N. ZHENG, K. MORIKUNI, AND J.-F. YIN, *Kaczmarz-type inner-iteration preconditioned flexible GMRES methods for consistent linear systems*, SIAM J. Sci. Comput., (accepted), p. <https://arxiv.org/abs/2006.10818>.
- [5] T. ELFVING AND P. C. HANSEN, *Unmatched projector/backprojector pairs: perturbation and convergence analysis*, SIAM J. Sci. Comput., 40 (2018), pp. A573–A591.
- [6] T. ELFVING, P. C. HANSEN, AND T. NIKAZAD, *Semi-convergence properties of Kaczmarz’s method*, Inverse Problems, 30 (2014), p. 055007.

- [7] D. C.-L. FONG, *LSMR: An iterative algorithm for least-squares problems*, 2021. available from mathworks.com/matlabcentral/fileexchange/27183-lsmr-an-iterative-algorithm-for-least-squares-problems.
- [8] D. C.-L. FONG AND M. SAUNDERS, *LSMR: An iterative algorithm for sparse least-squares problems*, SIAM J. Sci. Comput., 33 (2011), pp. 2950–2991.
- [9] S. GAZZOLA AND P. NOVATI, *Inheritance of the discrete Picard condition in Krylov subspace methods*, BIT Numer. Math., 56 (2016), pp. 893–918.
- [10] K. HAHN, H. SCHÖNDUBE, K. STIERSTORFER, J. HORNEGGER, AND F. NOO, *A comparison of linear interpolation models for iterative CT reconstruction*, Medical Physics, 43 (2016), pp. 6455–6473.
- [11] M. HANKE, *Conjugate Gradient Type Methods for Ill-Posed Problems*, Longman Scientific & Technical, Essex, 1995.
- [12] ———, *On lanczos based methods for the regularization of discrete ill-posed problems*, BIT, 41 (2001), pp. 1008–1018.
- [13] P. C. HANSEN, *Rank-Deficient and Discrete Ill-Posed Problems: Numerical Aspects of Linear Inversion*, SIAM, Philadelphia, 1998.
- [14] ———, *Regularization Tools version 4.0 for Matlab 7.3*, Numer. Algo., 46 (2007), pp. 189–194.
- [15] ———, *Discrete Inverse Problems: Insight and Algorithms*, SIAM, Philadelphia, 2010.
- [16] P. C. HANSEN AND J. S. JØRGENSEN, *AIR Tools II: algebraic iterative reconstruction methods, improved implementation*, Numerical Algorithms, 79 (2018), pp. 107–137.
- [17] P. C. HANSEN, J. S. JØRGENSEN, AND W. R. B. LIONHEART, eds., *Computed Tomography: Algorithms, Insight and Just Enough Theory*, SIAM, Philadelphia, 2021.
- [18] P. C. HANSEN, J. S. JØRGENSEN, AND P. W. RASMUSSEN, *Stopping rules for algebraic iterative reconstruction methods in computed tomography*, tech. rep., 2021. submitted to the workshop Application of Numerical Analysis to Imaging Science during the ICCSA 2021 conference, arXiv preprint [arXiv:2106.10053](https://arxiv.org/abs/2106.10053).
- [19] K. HAYAMI, J.-F. YIN, AND T. ITO, *GMRES methods for least squares problems*, SIAM J. Matrix Anal. Appl., 31 (2010), pp. 2400–2430.
- [20] C.-H. HUNG AND T. L. MARKHAM, *The Moore–Penrose inverse of a partitioned matrix $M = \begin{pmatrix} A & D \\ B & C \end{pmatrix}$* , Linear Algebra Appl., 11 (1975), pp. 73–86.
- [21] ———, *The Moore–Penrose inverse of a sum of matrices*, J. Aust. Math. Soc., 24 (1977), pp. 385–392.
- [22] T. JENSEN AND P. HANSEN, *Iterative regularization with minimum residual methods*, BIT, 47 (2007), pp. 103–120.
- [23] Z. JIA, *Regularization properties of Krylov iterative solvers CGME and LSMR for linear discrete ill-posed problems with an application to truncated randomized SVDs*, Numerical Algorithms, 85 (2020), pp. 1281–1310.
- [24] D. S. LALUSH AND M. N. WERNICK, *Iterative image reconstruction*, in Emission Tomography – The Fundamentals of PET and SPECT, M. N. Wernick and J. N. Aarsvold, eds., Elsevier, 2004.

- [25] K. MORIKUNI AND K. HAYAMI, *Convergence of inner-iteration GMRES methods for rank-deficient least squares problems*, SIAM J. Matrix Anal. Appl., 36 (2015), pp. 225–250.
- [26] V. A. MOROZOV, *Methods for Solving Incorrectly Posed Problems*, Springer, NY, 1984.
- [27] F. NATTERER, *The Mathematics of Computerized Tomography*, SIAM, Philadelphia, 2001 (reprint).
- [28] W. J. PALENSTIJN, K. J. BATENBURG, AND J. SIJBERS, *Performance improvements for iterative electron tomography reconstruction using graphics processing units (GPUs)*, J. Struct. Biol., 176 (2011), pp. 250–253.
- [29] L. REICHEL AND G. RODRIGUEZ, *Old and new parameter choice rules for discrete ill-posed problems*, Numer. Algo., 63 (2013), pp. 65–87.
- [30] H. H. B. SØRENSEN AND P. C. HANSEN, *Multicore performance of block algebraic iterative methods*, SIAM J. Sci. Comput., 36 (2014), pp. C524–C546.
- [31] G. W. STEWART AND J.-G. SUN, *Matrix Perturbation Theory*, Academic Press, Boston, 1990.
- [32] W. VAN AARLE, W. J. PALENSTIJN, J. CANT, E. JANSSENS, R. BLEICHRODT, A. DABRAVOLSKI, J. D. BEENHOUWER, K. J. BATENBURG, AND J. SIJBERS, *Fast and flexible X-ray tomography using the ASTRA toolbox*, Opt. Express, 24 (2016), pp. 25129–25147. available from astra-toolbox.com.
- [33] B. S. VAN LITH, P. C. HANSEN, AND M. E. HOCHSTENBACH, *A twin error gauge for Kaczmarz’s iterations*, SIAM J. Sci. Comput., special section Coppen Mountain 2020 (2021).
- [34] P.-Å. WEDIN, *Perturbation bounds in connection with singular value decomposition*, BIT, 12 (1972), pp. 99–111.